Transient Aeroelastic Response of a Rotor during Rotor Speed Transition in Forward Flight

Dong Han[1]

Nanjing University of Aeronautics and Astronautics, Nanjing, Jiangsu, 210016, China

and

George N. Barakos [2]

University of Glasgow, Glasgow, Scotland G12 8QQ, United Kingdom

Compound helicopters often have to reduce their rotor tip speeds to achieve higher forward speeds. The rotors, therefore, have to undergo a transient process of rotor speed changes. To investigate the transient loads and the related transformation from the rotating frame to the non-rotating frame, a rotor model is used to predict the transient aeroelastic responses. The rotor model is validated by using test data of a teetering model rotor during engagement and disengagement operations. The investigations indicate that a small transient lagwise root bending moment can result in a large transient contribution to rotor torque. This transient component is triggered by the force related with the sudden change of the angular acceleration of the rotor speed. Increasing the blade damping in the lagwise direction can significantly decrease the transient components of the lagwise root bending moment and the corresponding rotor torque. Making the angular acceleration continuous will not trigger the transient components, suggesting this is a better way for the reduction of the transient rotor loads during speed changes.

[1] Professor, College of Aerospace Engineering; donghan@nuaa.edu.cn (Corresponding Author).
[2] Professor, CFD Laboratory, School of Engineering; George.Barakos@glasgow.ac.uk.

Nomenclature

n = number of generalized degrees

N_b = number of rotor blades

Q = generalized force

q = generalized coordinate

t = time, s

V = velocity, m/s

θ_0 = collective pitch, rad

θ_{1c} = lateral cyclic pitch, rad

θ_{1s} = the longitudinal pitch, rad

ψ = azimuth, rad

Ω = rotor speed, rad/s

Superscript

A = contribution from aerodynamics

E = contribution from elastic potential energy

T = contribution from kinetic energy

$(\cdot)$ = d/dt

I. Introduction

The maximum forward speed of a helicopter is limited by advancing blade compressibility and retreating blade stall. Therefore, to increase the maximum forward speed of a helicopter, the blade tip speed may have to be reduced to alleviate compressibility effects. For high speed compound helicopters [1-3], tip speed is usually reduced in high speed flight, and at a specified forward speed, the rotor will undergo a transient process of rotor speed transition.

A change in the rotor speed may produce transient loads in the rotor system, which may be transferred to the rotor shaft or the fuselage. As known, an ideal rotor with identical blades acts like a filter [4, 5]. The excitations from the blades at the frequencies of $(N_b\text{-}1)\Omega$, $N_b\Omega$, $(N_b\text{+}1)\Omega$, $(2N_b\text{-}1)\Omega$, $2N_b\Omega$, $(2N_b\text{+}1)\Omega$, ⋯, can be transmitted to the fixed frame (rotor hub, fuselage) at the frequencies of $N_b\Omega$, $2N_b\Omega$, ⋯. This principle is true for steady rotor

loads. Whether the transfer of the transient loads from the rotating frame to the non-rotating frame follows this principle needs further investigation.

If large transient loads are transferred, the rotor shaft or the fuselage may be damaged, or more severe consequences may be caused. Large lagwise transient loads of a variable speed rotor during lagwise resonance crossing have been documented in [6, 7]. Chandrasekaran and Hodges investigated the performance and resonance dynamics of a variable speed rotor using geometrically exact beam formulations [8]. The research confirmed that the forces acting on the blade root increased significantly during a resonance crossing. During resonance crossing, it is natural that high transient loads appear. However, if the resonance is excluded from the range of the variation of the rotor speed, are there any other large transient loads?

During forward flight, conventional helicopters do not normally change their rotor speeds, and the changes of their rotor speeds are limited to a small range. Naturally, few researches focused on the transient aeroelastic response during the rotor speed transition in forward flight. Before take-off and after landing, the rotor speeds of helicopters have to increase from zero to nominal rotor speed, or the opposite. Several works already focused on this topic [9-13], and the blade deflection in the flapwise direction may result in the blade accidentally hitting the fuselage, ground, or ship deck [14]. These investigations indicated that the transient aeroelastic response may be severe during the variation of rotor speed.

This work focuses on the analysis of the transient aeroelastic response of a rotor during rotor speed transition in forward flight, and considers the loads transfer from the rotating frame to the non-rotating frame. A validated rotor model is used to predict the transient aeroelastic responses during rotor speed transition. To reduce the transient loads, adding damping to rotor blades and changing the strategy of the rotor speed variation are discussed to investigate the effectiveness of these methods.

II. Modeling Method

A. Modeling

The rotor model used in this work follows earlier efforts [12, 15]. A moderate deflection beam model is employed to describe the elastic deformations of rotor blades. Rigid rotations associated with blade hinges and rotor rotations are introduced based on a generalized force formulation [16]. A nonlinear quasi-steady aerodynamic model

with table look-up aerofoil aerodynamics is used to describe the blade aerodynamics. The induced velocity over the rotor disk in both steady and transient states is captured by the Pitt-Peters dynamic inflow model [17].

According to Hamilton's principle, the implicit nonlinear dynamic equations include three parts: elastic potential energy, kinetic energy, and work done by the aerodynamics. For an articulated or hingeless rotor, all the blades share the degree of **freedom of** rotation around the rotor shaft (rotor speed, Ω). The equations of motion based on the generalized force formulation for the rotor can be expressed as

$$Q_j^T\left(\mathbf{q}_1, \dot{\mathbf{q}}_1, \ddot{\mathbf{q}}_1, \cdots, \mathbf{q}_{\mathrm{i}}, \dot{\mathbf{q}}_{\mathrm{i}}, \ddot{\mathbf{q}}_{\mathrm{i}}, \cdots \mathbf{q}_{\mathrm{N_b}}, \dot{\mathbf{q}}_{\mathrm{N_b}}, \ddot{\mathbf{q}}_{\mathrm{N_b}}, t, \Omega, \dot{\Omega}\right) + Q_j^E\left(\mathbf{q}_1, \dot{\mathbf{q}}_1, \ddot{\mathbf{q}}_1, \cdots, \mathbf{q}_{\mathrm{i}}, \dot{\mathbf{q}}_{\mathrm{i}}, \ddot{\mathbf{q}}_{\mathrm{i}}, \cdots \mathbf{q}_{\mathrm{N_b}}, \dot{\mathbf{q}}_{\mathrm{N_b}}, \ddot{\mathbf{q}}_{\mathrm{N_b}}, t, \Omega, \dot{\Omega}\right)$$
$$+ Q_j^A\left(\mathbf{q}_1, \dot{\mathbf{q}}_1, \ddot{\mathbf{q}}_1, \cdots, \mathbf{q}_{\mathrm{i}}, \dot{\mathbf{q}}_{\mathrm{i}}, \ddot{\mathbf{q}}_{\mathrm{i}}, \cdots \mathbf{q}_{\mathrm{N_b}}, \dot{\mathbf{q}}_{\mathrm{N_b}}, \ddot{\mathbf{q}}_{\mathrm{N_b}}, t, \Omega, \dot{\Omega}\right) = 0$$
$$(j = 1,2,\cdots,(n-1)N_b + 1) \quad (1)$$

where, **q** denotes the generalized degrees of freedom used to describe a single blade, and i denotes a blade. Since all the blades just share a degree of freedom, $N_b - 1$ degrees of freedom are constrained in the system. The fifteen degree-of-freedom beam element is utilized to discretize the blades [18]. The implicit Newmark integration method is utilized to calculate the steady and transient responses in the time domain [19].

B. Modeling Validation

Newman [9] investigated the dynamic responses of a teetering model rotor on a model ship in a wind tunnel during engagement and disengagement operations. The wind came from the 90^o direction orthogonal to the centerline of the ship. The test data was obtained at five locations (A, B, C, D and E) in the lateral direction on the ship deck, as shown in Figure **1(e).** When the test began, the rotor speed was 0rpm. **At** 42s, the rotor speed was **linearly incremented** to 600rpm, to simulate the engagement operation. Then, the rotor speed was maintained for 6s to simulate steady operation. At last, the rotor speed was **linearly** reduced to 0rpm in 10s, which was utilized to model the disengagement operation. The time histories of the teeter angle with and without turbulence and the rotor speed are shown in Figure 1. The predictions using the present method are in good agreement with the test data [8] and the predictions by Keller [13]. The comparisons indicate that the present model can be used to analyze the transient aeroelastic responses of helicopter rotors, as the rotor speed varies.

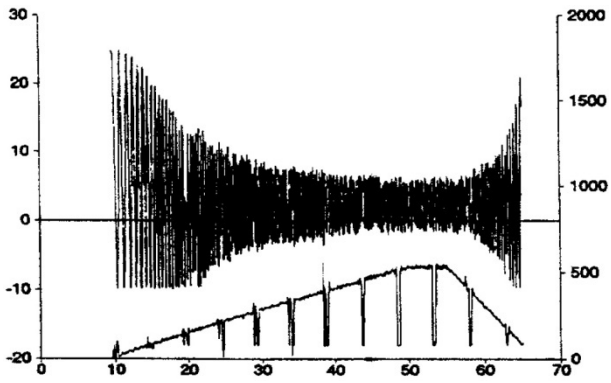

(a) Test data [8]

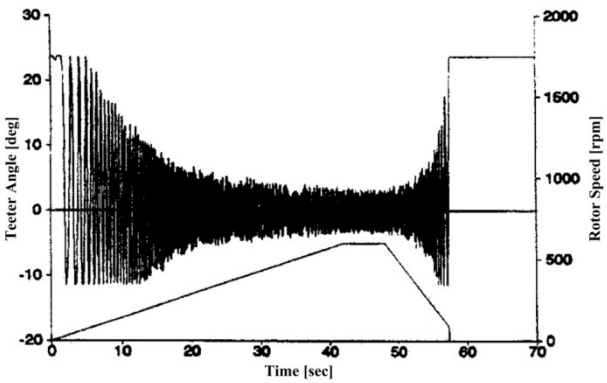

(b) Prediction [8]

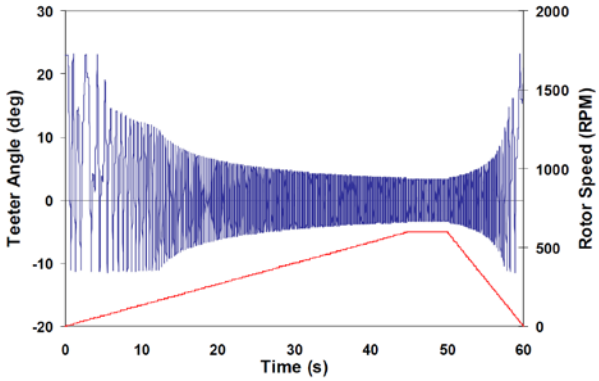

(c) Prediction **without turbulence** [13]

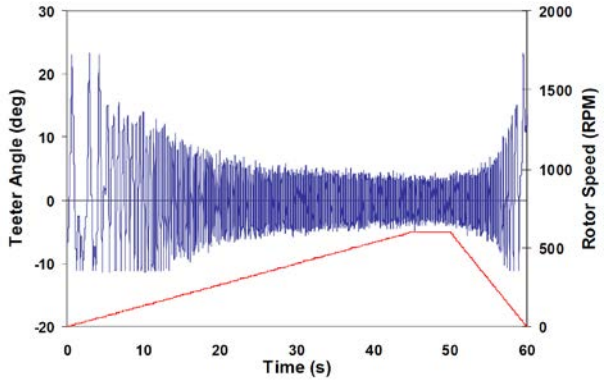

(d) Prediction with **a turbulence intensity of 0.2** [13]

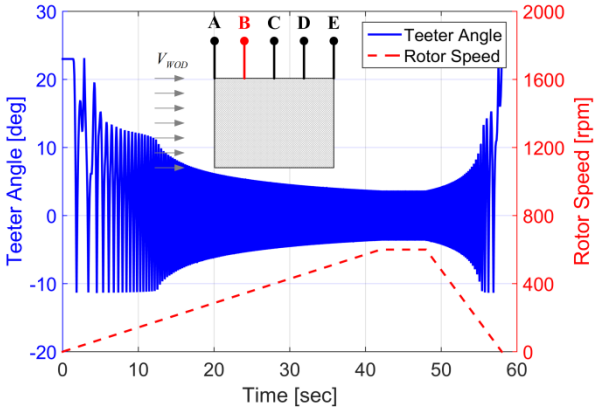

(e) Present prediction **without turbulence**

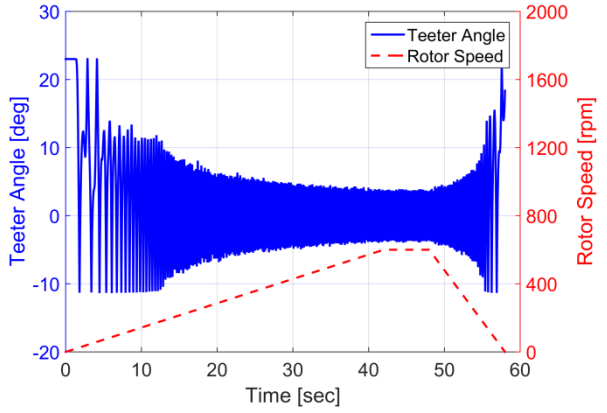

(f) Present prediction **with a turbulence intensity of 0.2**

Figure 1 The transient responses at location B.

III. Transient Response

The transient aeroelastic responses are calculated for all blades simultaneously, and the rotor hub forces and moments are derived from the resultant forces and moments of the root forces and moments of all rotor blades. Inherent system damping of 1% critical is included in the fundamental lag mode to represent the intrinsic low levels of structural damping. The time histories of the rotor speed and the corresponding angular acceleration are prescribed during the rotor speed transition in forward flight. To maintain the rotor thrust and forward speed, the pitch changes need to be provided to the rotor. A dynamic wind-tunnel trim is utilized to provide the time histories of the pitch controls. The pitch controls in steady state for several discrete rotor speeds are trimmed to the same thrust, 1/rev rotor flapping, and forward speed. During the variation of the rotor speed, the pitch controls between two adjacent rotor speeds are calculated by using linear interpolation.

A. Baseline Rotor

The XH-59A helicopter rotor is adopted as a representative rotor. The parameters of the rotor are listed in Table 1, and the blade property can refer to [20-22]. The stiffness properties of the rotor blade are shown in Figure 2. The airfoils of the rotor blades are changed to NACA0012. The nominal blade tip speed of the XH-59A at helicopter mode is 198.12 m/s, and the corresponding rotor speed Ω is 345rpm (5.75Hz). For the high-speed mode (aircraft mode) above 296.32 km/h, the tip speed is reduced to alleviate the compressibility effect. Therefore, the tip speed is changed to 137.16 m/s [22], and the corresponding rotor speed is 239rpm (3.98Hz, 69.23%Ω). The predicted rotor blade frequencies at the helicopter and aircraft modes are listed in Table 2. ‘F’ denotes a flapwise frequency; ‘L’ denotes a lagwise frequency and ‘T’ denotes a torsional frequency. At the helicopter mode, the 2nd lagwise frequency ratio of the blade is close to 6.0, which indicates that the 6/rev blade lagwise load may be large. For this three-bladed rotor, this harmonic load can be transferred to the rotor shaft, which may cause severe vibration in the transmission system.

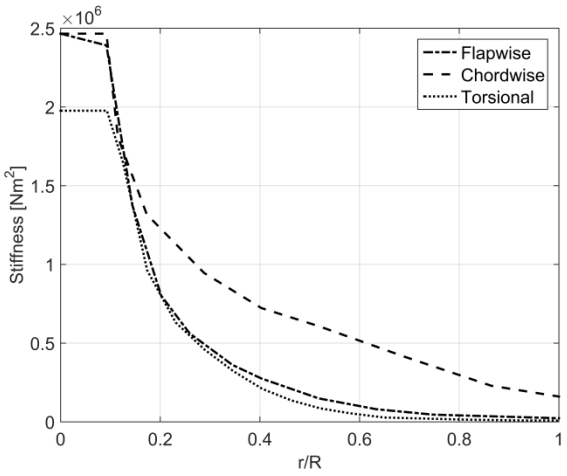

Figure 2 Stiffness properties of the rotor blade.

Table 1 XH-59A rotor parameters

Parameters	Value
Rotor type	Hingeless
Rotor radius, R	5.4864 m
Number of rotor blades, N_b	3
Blade tip chord	0.2859 m
Blade taper ratio	2:1
Blade twist (nonlinear)	-10 deg
Blade precone angle	3 deg
Designed rotor tip speed, ΩR	198.12 m/s

Table 2 Blade frequency ratios at different rotor speeds

Mode	100%Ω	69.3%Ω
F1	1.41	1.56
F2	4.22	5.32
L1	1.23	1.70

L2	5.92	8.17
T1	11.26	16.29

B. Transient Response during Rotor Speed Transition

The XH-59A helicopter has to reduce the rotor speed from 100%Ω to 69.3%Ω at a very high speed. To investigate the dynamic behavior of the rotor during the rotor speed transition, a forward speed of 300km/h is set as the transition speed, and the rotor speed varies linearly as **follows**

$$\begin{cases} \Omega_1 & t < t_1 \\ \Omega_1 + \dfrac{t - t_1}{t_2 - t_1}(\Omega_2 - \Omega_1) & t_1 \le t \le t_2 \\ \Omega_2 & t_2 \le t \end{cases} \tag{2}$$

where, Ω_1 is the rotor speed at the beginning of the transition (100%Ω), and Ω_2 is the rotor speed at the end of the transition (69.3% Ω). t_1 is the beginning time of the transition, and t_2 is the end time. In the following analysis, the transition begins at $t_1 = 5$s, and ends at $t_2 = 25$s. The transient process lasts 20s. The time histories of the rotor speed and the corresponding angular acceleration are shown in Figure 3. **As a consequence, stepwise** changes in the angular acceleration appear at the beginning and end of the transition.

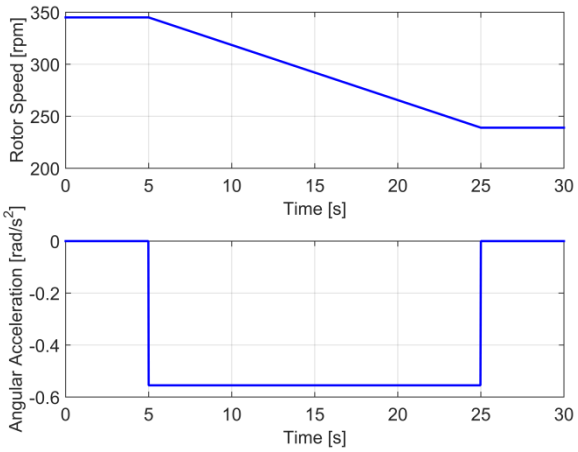

Figure 3 Time histories of the rotor speed and the corresponding angular acceleration.

An isolated rotor is used to analyze the transient process. The rotor thrust remains at 12250N, and the longitudinal and lateral blade flappings are trimmed to be 0^o for the wind-tunnel trim. The time histories of the

collective pitch θ_0, the lateral cyclic pitch θ_{1c} and the longitudinal pitch θ_{1s} are shown in Figure 4. A lower rotor speed leads to larger pitch controls.

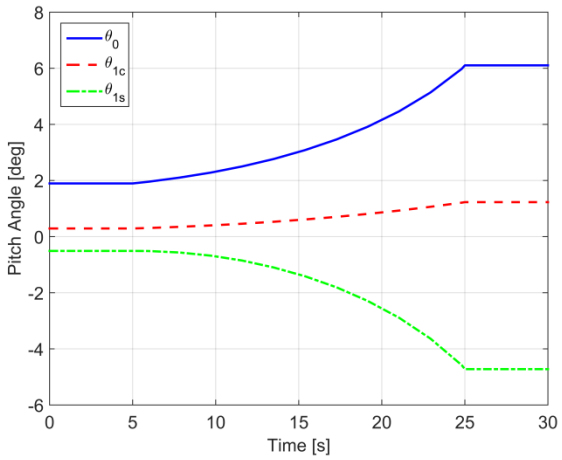

Figure 4 Time histories of the pitch controls.

Figure 5 shows the time history of the flapwise root bending moment of a blade. The variation is relatively smooth, and there are no sudden changes in the flapwise moment during the transition. **When a** steady state **condition is reached**, with a lower rotor speed **at $t > 25$s**, a peak-peak moment larger than that at a higher rotor speed**, for $t < 5$s, is observed**. Figure 6 shows the time history of the rotor thrust. It is clear that the rotor thrust remains relatively smooth, and the average value is 12250N.

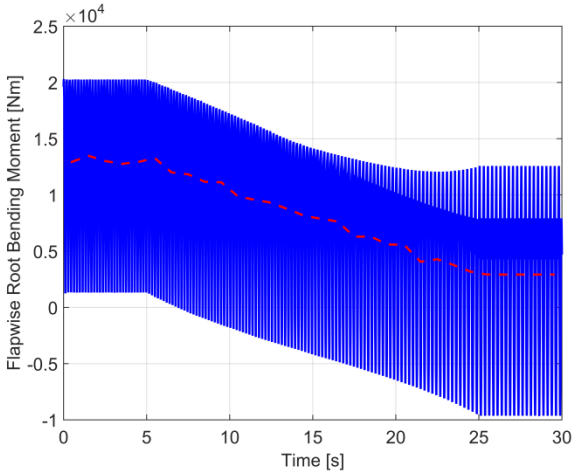

Figure 5 Time history of the blade flapwise root bending moment.

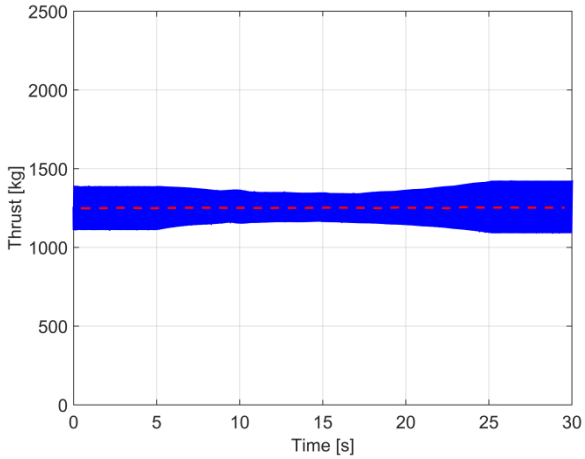

Figure 6 Time history of the rotor thrust.

Figure 7 shows the time history of the lagwise root bending moment of the blade. Different from the flapwise moment in Figure 5, a sharp rise appears right after the beginning of the transition. The FFT (Fast Fourier Transform) analysis of the response from 5s to 9.905s is shown in Figure 8. The frequency of the largest component is approximately equal to the baseline rotor speed. The frequency of the next component is approximately equal to the natural frequency of the 1st lagwise blade mode at the rotor speed of 345 rpm. This transient component is excited at the beginning of the transition. The FFT analysis of the response from 25s to 29.905s is shown in Figure 9. The frequency of the 1st harmonic component is approximately equal to the rotor speed of 239rpm. The frequency of the 2nd component is not easy to be distinguished in the figure, and is approximately equal to the frequency of the 1st lagwise mode at the rotor speed of 239rpm. The frequency of the largest harmonic component is about 2 times the rotor speed of 239rpm. At the beginning and the end of the transient process, the transient components corresponding to the 1st lagwise blade mode are excited. Lowering the rotor speed leads to a significant increase in the 2/rev lagwise root bending moment. **As illustrated in [15], the frequency ratio of the 1st lagwise mode changing from 1.23 to 1.70 can contribute to the increase in the 2/rev lagwise root bending moment. In addition, due the coupling between the flap and lag modes [6], the change in the blade flapping due to the reduction of rotor speed can also contribute to the increase.**

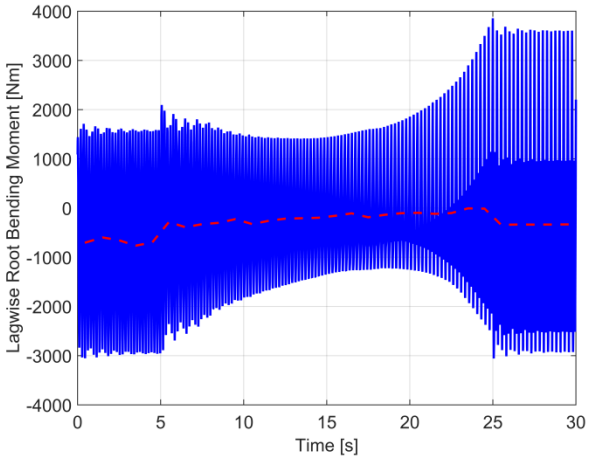

Figure 7 Time history of the lagwise root bending moment.

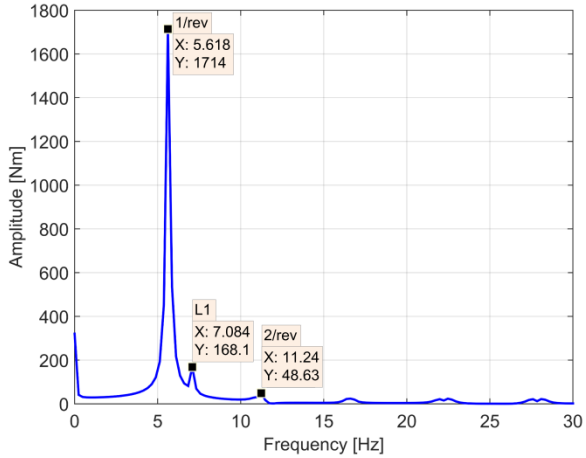

Figure 8 FFT analysis of the lagwise root bending moment from 5s to 9.095s.

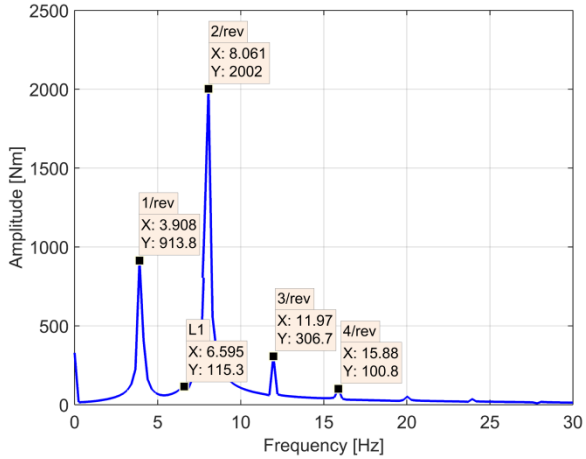

Figure 9 FFT analysis of the lagwise root bending moment from 25s to 29.095s.

Figure 10 shows the time history of the rotor torque. The transient components of the rotor torque appear at the beginning and end of the transition. Figure 11 shows the FFT analysis of the response during 5s to 9.095s. The frequency of the largest harmonic (1st harmonic component) is equal to the natural frequency of the 1st lagwise mode. This means that the transient component of the lagwise root bending moment is transferred to the rotor shaft. The frequency of the 2nd harmonic component is about 3.0 times the rotor speed of 345 rpm. For the three-bladed rotor, it will naturally be transferred to the rotor shaft. The frequency of the 3rd harmonic component is about 6.0 times the rotor speed of 345rpm. This component is unusually large, due to the frequency ratio of the 2nd lagwise mode approaching 6. Figure 12 shows the FFT analysis of the response from 25s to 29.095s. The frequency of the 1st harmonic component is equal to the natural frequency of the 1st lagwise blade mode at that rotor speed. The transient component is transferred to the rotor shaft. Obviously, the 2nd component is from the 3/rev component of the lagwise root bending moment.

The transient components in the lagwise root bending moment (2nd harmonic in Figure 8, 2nd harmonic in Figure 9) were small during the transient process. However, they were transferred to the rotor shaft, and resulted in large transient rotor torque (1st harmonic in Figure 11, 1st harmonic in Figure 12).

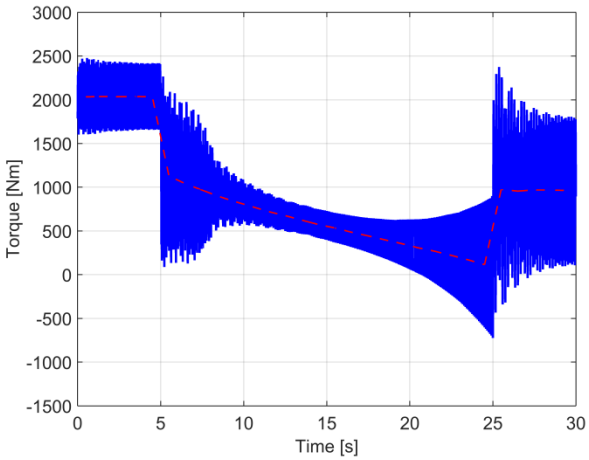

Figure 10 Time history of the rotor torque.

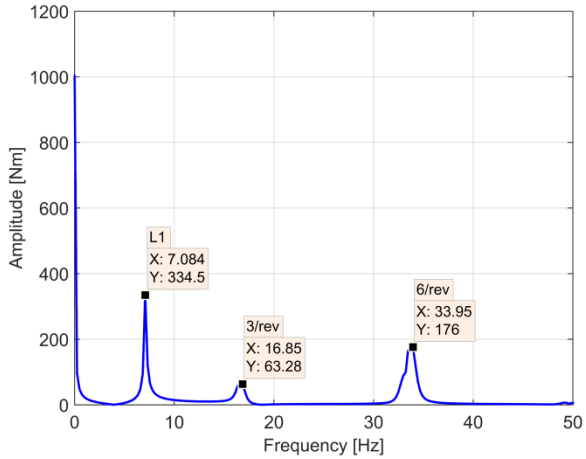

Figure 11 FFT analysis of the **rotor torque** from 5s to 9.095s

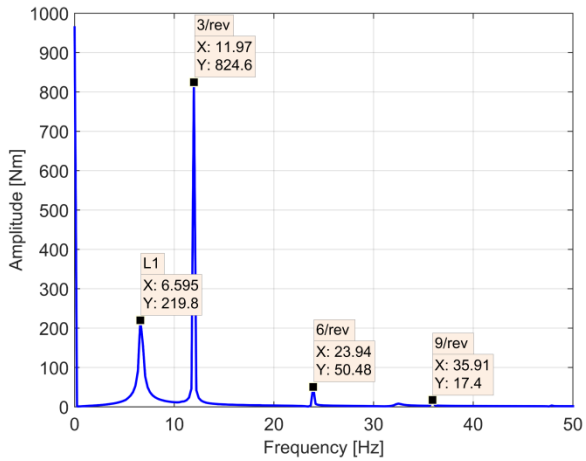

Figure 12 FFT analysis of the rotor torque from 25s to 29.095s

C. Transient Loads Reduction

Increasing the blade damping in the lagwise direction is an effective means to control the transient response [7]. The structural damping of the blade in the lagwise direction is increased from 1% to 5% critical damping. Figure 13 shows the time history of the lagwise root bending moment with the 5% critical damping. Compared with Figure 7, the transient responses at the beginning and end of the transition are significantly decreased. Figure 14 shows the time history of the corresponding rotor torque. Compared with Figure 10, not only the transient response, but also the steady response are significantly reduced. It is clear that increasing the blade damping is an effective means to control the transient response. However, adding damping to a rigid rotor is not an easy task.

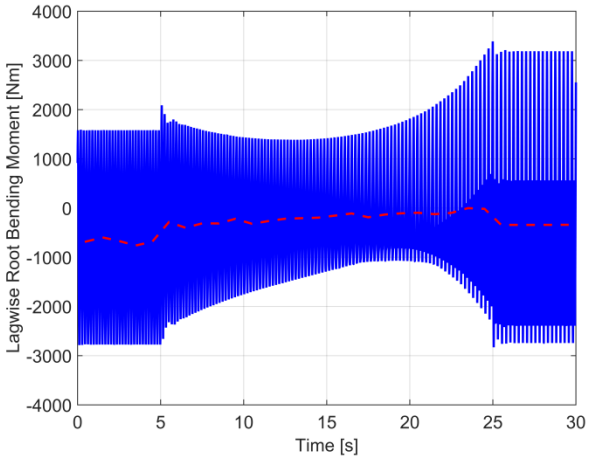

Figure 13 Time history of the lagwise root bending moment with 5% critical damping.

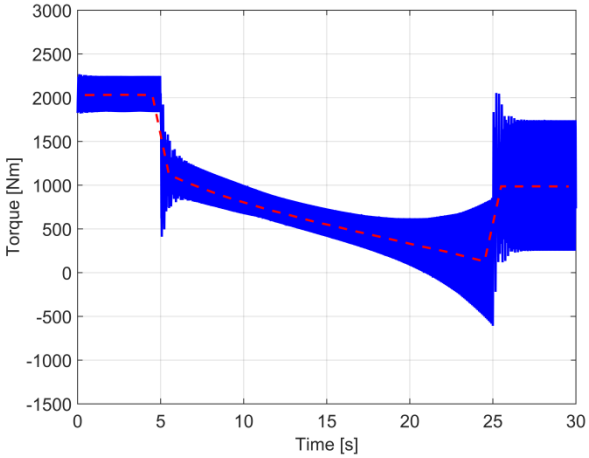

Figure 14 Time history of the rotor torque with 5% critical damping.

Figure 3 indicated that, the rotor speed is continuous, and the angular acceleration has sudden changes at the beginning and end of the transient process. These sudden changes can trigger the transient components of the lagwise root bending moment. In order to make the angular acceleration continuous, the strategy of the variation of the rotor speed is set as

$$\begin{cases} \Omega_1 & t < t_1 \\ \Omega_1 + \dfrac{\Omega_2 - \Omega_1}{2}\left[\cos\left(\dfrac{t - t_1}{t_2 - t_1}\pi + \pi\right) + 1.0\right] & t_1 \le t \le t_2 \\ \Omega_2 & t_2 \le t \end{cases} \tag{3}$$

Figure 15 shows the time histories of the rotor speed and corresponding angular acceleration using the new strategy. It is clear that the rotor speed and angular acceleration are continuous with time.

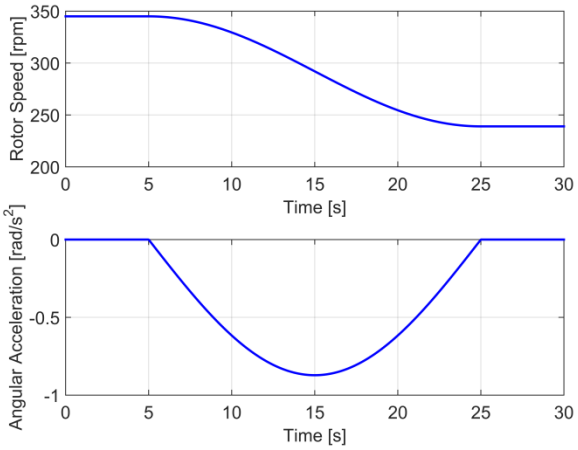

Figure 15 Time history of the rotor speed and the corresponding angular acceleration for the new strategy.

Figure 16 shows the time history of the lagwise root bending moment. The transient components at the beginning and end of the transition disappear, which indicates that the transient components are caused by the sudden changes of the angular acceleration. If the angular acceleration can vary continuously with time, the transient components will not be triggered. Figure 17 shows the time history of the corresponding rotor torque. The transient components at the beginning and end of the transition also disappear. Compared with Figure 14, the transient components decrease significantly. Increasing the blade damping can reduce the transient components, but cannot remove them. Making the angular acceleration continuous will not trigger the transient components, which is a better way for the control of the transient rotor torque.

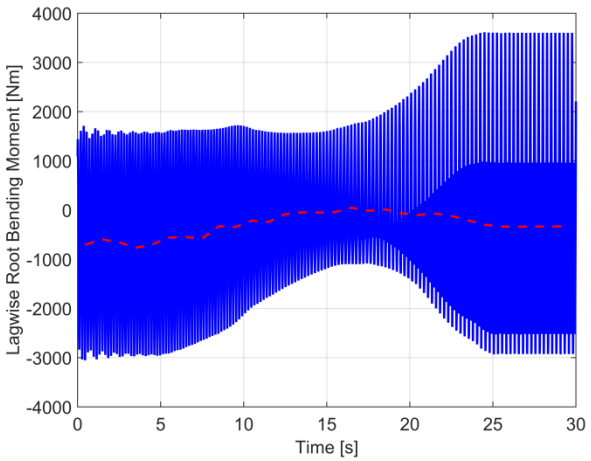

Figure 16 Time history of the lagwise root bending moment with the new strategy.

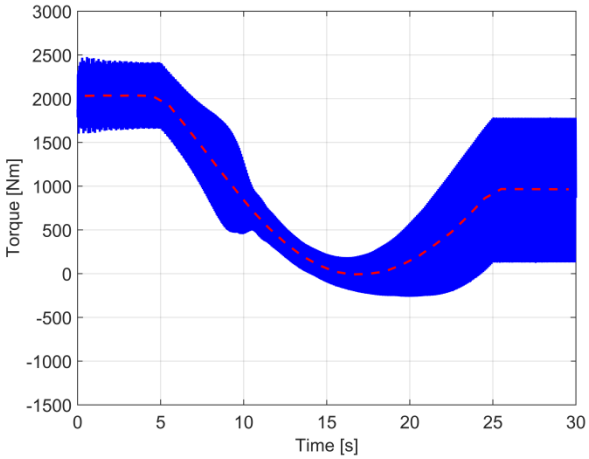

Figure 17 Time history of the rotor torque with the new strategy.

IV. Conclusion

This work focuses on the analysis of the transient aeroelastic response of a rotor during a rotor speed transition in forward flight. A rotor model is used to predict the transient aeroelastic responses of the flapwise and lagwise root bending moments and the corresponding rotor thrust and rotor torque. The analyses yielded the following conclusions:

1) A small transient lagwise root bending moment can lead to a large transient component of rotor torque. This transient component is **triggered** by the sudden change of the angular acceleration.

2) Increasing the blade damping in the lagwise direction can significantly decrease the transient components of the lagwise bending moment and the corresponding rotor torque.

3) The continuous change of angular acceleration will not trigger the transient components, making it a better way for the reduction of the transient loads.

4) The transient blade lagwise root bending moment with the damped natural frequency can be transferred to the rotor shaft.

Funding Sources

This work is supported from the National Natural Science Foundation of China (11972181), the Open Research Foundation of the Key Rotor Aerodynamics Laboratory (RAL20200104), and the Six Talent Peaks Project in Jiangsu Province (GDZB-013).

References

[1] Blackwell, R. and Millott, T., "Dynamics Design Characteristics of the Sikorsky X2 Technology™ Demonstrator Aircraft, 64th AHS Annual Forum, Montreal, Canada, April 29- May 1, 2008.

[2] Öhrle, C., Frey, F., Thiemeier, J., Keßler, M., Krämer, E., Embacher, M., Cranga, P., Eglin, P., "Compound Helicopter X3 in High-Speed Flight: Correlation of Simulation and Flight Test," 75th AHS Annual Forum, Philadelphia, Pennsylvania, May 13-16, 2019.

[3] Sugawara, H., and Tanabe, Y., "Numerical Investigation of Rotor/Wing Aerodynamic Interaction at High Advance Ratios," Journal of Aircraft, Vol. 56, No. 6, 2019, pp. 2285-2298.
DOI: 10.2514/1.C035370

[4] Reichert, G., "Helicopter Vibration Control - a Survey," Vertica, Vol. 5, No. 1, 1981, pp. 1-20.

[5] Johnson, W., Rotorcraft Aeromechanics, Cambridge University Press, New York, NY, USA, 2013, Chapter 18.
DOI: https://doi.org/10.1017/CBO9781139235655

[6] Han, D. and Smith, E. C., "Lagwise Dynamic Analysis of a Variable Speed Rotor," Aerospace Science and Technology, Vol. 29. No. 1, 2013, pp. 277-286.
DOI: 10.1016/j.ast.2013.03.010

[7] Han, D., Wang, J., Smith, E. C. and Lesieutre, G. A., "Transient Loads Control of a Variable Speed Rotor during Resonance Crossing," AIAA Journal, Vol. 51, No. 1, 2013, pp. 20-29.
DOI: 10.2514/1.J050598

[8] Chandrasekaran, R., and Hodges, D. H., "Performance advantages and resonance analysis of a variable speed rotor using geometrically exact beam formulations," 77th AHS Annual Forum, virtual conference, May 10-14, 2021.

[9] Newman, S. J., "The Verification of a Theoretical Helicopter Rotor Blade Sailing Method by Means of Windtunnel Testing," Aeronautical Journal, Vol. 99, No. 982, 1995, pp. 41-51.

[10] Geyer, W. P., Smith, E. C. and Keller, J. A., "Aeroelastic Analysis of Transient Blade Dynamics during Shipboard Engage/Disengage Operations," Journal of Aircraft, Vol. 35, No. 3, 1998, pp. 445-453.

[11] Wall, A. S., Afagh, F. F., Langlois, R. G. and Zan, S. J., "Modeling Helicopter Blade Sailing: Dynamic Formulation and Validation," Journal of Applied Mechanics, Transactions ASME , Vol. 75, No. 6, 2008,

pp. 0610041-06100410.

DOI: 10.1115/1.2957599

[12] Han, D., Wang, H.-W. and Gao, Z., “Aeroelastic Analysis of a Shipboard Helicopter Rotor with Ship Motions during Engagement and Disengagement Operations,” Aerospace Science and Technology, Vol. 16, No. 1, 2012, pp. 1-9.

DOI: 10.1016/j.ast.2011.02.001

[13] Zhang, J., Smith, E. C., Zajaczkowski, F., “Analysis of Rotor Start-Up and Shutdown on a Sea-Based Oil Rig,” Journal of Aircraft, Vol. 54, No. 1, 2017, pp. 20-35.

DOI: 10.2514/1.C033467

[14] Keller, J. A., “Analysis and Control of the Transient Aeroelastic Response of Rotors during Shipboard Engagement and Disengagement Operations,” Ph.D thesis, The Penn State University, 2001.

[15] Han, D. and Smith, E. C., “Lagwise Loads Analysis of a Rotor Blade with an Embedded Chordwise Absorber,” Journal of Aircraft, Vol. 46. No. 4, 2009, pp. 1280-1290.

DOI: 10.2514/1.40569

[16] Zheng, Z. C., Ren, G. and Cheng, Y. M., “Aeroelastic Response of a Coupled Rotor/Fuselage System in Hovering and Forward Flight,” Archive of Applied Mechanics, Vol. 69, No. 1, 1999, pp. 68-82.

DOI: 10.1007/s004190050205

[17] Peters, D. A., and HaQuang, N., “Dynamic Inflow for Practical Application,” Journal of the American Helicopter Society, Vol. 33, No. 4, 1988, pp. 64–68.

[18] Sivaneri, N. T and Chopra, I., “Finite Element Analysis for Bearingless Rotor Blade Aeroelasticity,” Journal of the American Helicopter Society, Vol. 29, No. 2, 1984, pp. 42 - 51.

DOI: 10.4050/jahs.29.42

[19] Owen, D. R. J. and Hinton, E., Finite Elements in Plasticity: Theory and Practice, Pineridge Press, Swansea, U.K., 1980: chapter 11.

[20] Felker, F. F., “Performance and Loads Data from a Wind Tunnel Test of a Full-Scale, Coaxial Hingeless Rotor Helicopter,” NASA TM 81239, 1981.

[21] Ruddell, A. J., “Advancing Blade Concept (ABC) Technology Demonstrator,” USAAVRADCOM-TR-81-D-5, 1981.

[22] Go, J.-I., Kim, D.-H., and Park, J.-S., “Performance and Vibration Analyses of Lift-Offset Helicopters,” International Journal of Aerospace Engineering, Vol. 2017, 2017, pp. 1865751.
DOI: 10.1155/2017/1865751